Revisiting the role of hydrogen bonding in the strong dimer superexchange of a 2D copper(II) halide honeycomb-like lattice: Structural and magnetic study

Jeffrey C. Monroe,*[a] M. Angels Carvajal,[b] Mercè Deumal,*[b] Christopher P. Landee,[c] Melanie Rademeyer[d] and Mark M. Turnbull*[a]

[a]*Carlson School of Chemistry and Biochemistry, Clark University, 950 Main St., Worcester, MA 01610 USA.* [b]*Dept. Ciència de Materials i Química Física, & IQCTUB, Universitat de Barcelona, Martí i Franquès 1, Barcelona, E-08028.* [c]*Department of Physics, Clark University, 950 Main St., Worcester, MA 01610 USA.* [d]*Department of Chemistry, University of Pretoria, Private Bag X20, Hatfield 0028, South Africa.*

Abstract:

The title compound $H_2L(CuCl_3H_2O)Cl$ H_2L=*1-(4'-Pyridinium)pyridin-4-ol-ium)* (**1**) was synthesized and investigated structurally and magnetically as well as via a First-Principles Bottom-Up theoretical analysis of the potential magnetic superexchange pathways. Compound **1** can be described structurally as a well isolated, distorted 2D-honeycomb lattice with two potential exchange pathways: a dimeric interaction via hydrogen bonded pairs of ($CuCl_3H_2O$) ions and a chain structure via bridging chloride ions. Surprisingly, the experimental magnetic data are best fitted using both a simple dimer model with a Curie-Weiss correction for interdimer exchange (J_{dimer} = -107.4(1) K, θ = -1.22(4) K) and a strong-rung ladder model (J_{rung} = -105.8(7) K, J_{rail} = 2(7) K). Theoretical analysis at the UB3LYP/6-31+G(d) level supports the strong exchange observed through the $[CuCl_4(H_2O)]^{2-}$ dimer moiety superexchange pathway (−102 K = −71 cm^{-1}). However, the apparent vanishingly small exchange through the single halide bridge is merely a brute average of competing FM (+24.8 K = +17.0 cm^{-1}) and AFM (−21.0 K = −14.6 cm^{-1}) exchange interactions. Our computational study shows that these fitting parameters carry no physical meaning since a honeycomb plaquette must be taken as magnetic building block for **1**. The competition between FM and AFM pair interactions leads to geometrical frustration in **1** and could induce interesting magnetic response at low temperatures, if the magnetic exchange is adequately tuned by modifying substituents in ligands and, in turn, interactions within the crystal packing.

Introduction:

Renewed interest in the magnetic properties of low-dimensional transition metal lattices followed the discovery of low-dimensional superexchange (2D) in the high temperature copper oxide superconductors.[1,2,3,4] Thus, over the course of three decades, the synthesis of low-dimensional copper(II) lattices has been a major focus of attempts to understand the effects of structure on the magnitude and sign

of the superexchange and to study the ground state behavior and long range order (LRO) in these quantum dominated systems. It has been subsequently found that interesting quantum effects are observed depending on the interaction topology in the ground state of such low-dimensional systems.[5,6,7] The 2D-Quantum Heisenberg antiferromagnetic (2D-QHAF) square lattice, for instance, has a mixed ground state and achieves long range order at a temperature proportional to J'/J where J' is the interlayer exchange and J is the intralayer exchange.[8] For $J' = 0$, the 2D-QHAF model orders at T = 0 K, while at finite temperatures thermal fluctuations hinder ordering. One robust approach[9,10,11,12,13,14,15] toward achieving such 2D lattices is to synthesize salts of the type $(HL)_2CuX_4$ where HL is a protonated organic base, such as a substituted pyridine-based cation, and X is chloride or bromide. In these complexes, the HL ions pack such that CuX_4 layers may be well isolated, giving the desired 2D superexchange which may be comprised of two-halide exchange pathways.[8,11] Investigation of many such lattices allows the construction of magnetostructural correlations toward understanding the nature of superexchange and ordering phenomena. For instance, the magnitude and sign of J through a two-halide pathway[11,16] has been qualitatively related to the distance X···X and the torsion angle Cu-X···X-Cu where short X···X distances and torsion angles near 0° and 180° give strong superexchange. While much work in this field exists, there is a strong push towards synthesizing more diverse structures which may contain unique or interesting superexchange pathways and topologies. For instance, the difficult-to-synthesize[6] honeycomb lattice is well studied theoretically because a number of quantum effects may dominate the ground state depending on slight deviations from an isotropic Heisenberg system, including the sought after quantum spin liquid phase.[5,17,18,19,20,21]

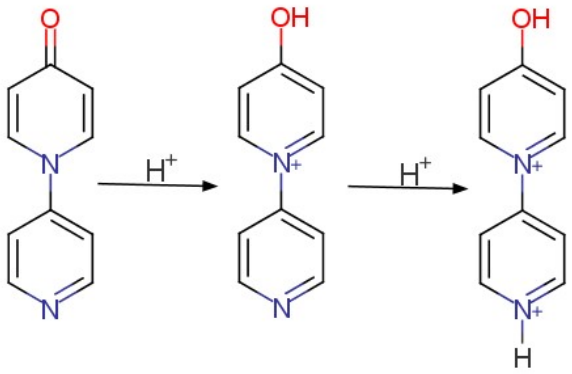

L **HL$^+$** **H$_2$L^{2+}**

Figure 1. Forms of the molecule **L**, (1-(4'-pyridyl)-4-pyridone), from treatment with protic acid.

In an attempt to provide a structurally diverse family of copper(II) lattices, compounds with **L**, **HL$^+$** and **H$_2$L^{2+}** are under study (Figure 1). The neutral ligand **L** is ambidentate and may coordinate a

transition metal via the pyridone oxygen atom, or the pyridine nitrogen atom[22,23,24,25,26] and the monoprotonated specie $\mathbf{HL^+}$ may behave in similar fashion, although coordination of the protonated oxygen atom is less likely. The doubly protonated molecule, $\mathbf{H_2L^{2+}}$, may provide charge balance for a CuX_4^{-2} moiety and control the lattice formation through hydrogen bonding. However, it is no longer a good candidate as a ligand as there are no available coordination sites. Our group has proposed that use of this versatile trio of compounds may give structurally diverse complexes because of the unusual charge balance motif and the potential to evaluate existing magneto-structural correlations via investigation of the likely large family of such. Here we report the results of our initial investigation in applications of $\mathbf{H_2L^{2+}}$, the synthesis, structure, magnetic and theoretical characterization of $H_2L[CuCl_3(H_2O)]Cl$ (**1**).

Experimental

Materials and Methods:

4-Hydroxypyridine was purchased from Alfa Aesar and $CuCl_2{\cdot}2H_2O$ from Allied Chemical Corporation; both were used as received. Elemental analysis was performed at the Marine Science Institute, University of California Santa Barbara, CA. The infrared spectrum was collected using a Perkin Elmer FT-IR 100 spectrometer on a powdered sample.

1-(4'-Pyridyl)pyridin-4-one dihydrate: The ligand 1-(4'-pyridyl)pyridin-4-one dihydrate was synthesized similarly to the literature procedure.[27] A neat mixture of acetic anhydride (124 mmol, 12.63 g) with 4-hydroxypyridine (53 mmol, 5.03 g) was refluxed while stirring under N_2 atmosphere for 5 hours. The resulting brown reaction mixture was allowed to cool while stirring and eventually solidified. The solid was triturated with diethyl ether and then filtered giving the brown crude product. The crude product was recrystallized from toluene giving yellowish needles (1.83 g, 33% yield). NMR ^{1}H solvent: D_2O (ppm) 8.72 (doublet J = 1.46 Hz), 8.2 (doublet J = 2.2 Hz), 7.65 (doublet J = 1.62 Hz), 6.35 (doublet J = 2 Hz). IR ν (cm^{-1}): 3232 (br, db), 3037 (w, mult), 1633 (s), 1588 (sh), 1568 (s, db), 1496 (s), 1410 (m), 1355 (m), 1331 (w), 1288 (s), 1223 (m), 1198 (s), 1070 (w), 1028 (m), 996 (w), 844 (sh, m), 829 (s), 717 (m) (s = strong, m = medium, w = weak, db = double, mult = multiple, br = broad, sh = shoulder, v = very). The ^{1}H-NMR spectrum is shown in Supporting Information Section 1.

1-(4'-Pyridinium)pyridin-4-ol-ium) aquatrichlorocopper(II) chloride **(1):** 1-(4'-Pyridyl)pyridin-4-one dihydrate (419 mg, 2.00 mmol) was dissolved in HCl (6 M, 10 ml) giving a yellow solution. $CuCl_2{\cdot}2H_2O$ (175 mg, 1 mmol) was dissolved in H_2O (5 ml) giving a blue solution which was added to the acid solution, turning it green. This solution was filtered and left to slowly evaporate at room temperature; it became yellow as it concentrated. After four days, green hexagonal crystals of **1** were picked from solution with a spatula and dried mechanically (0.264 g, 65%). Attempts to wash the crystals with a variety of solvents caused degradation. Calc'd CHN: C (30.21%) H (3.04%) N (7.05%). Found CHN: C (30.59%) H (2.99%)

N (7.07%). IR ν (cm^{-1}): 3326 (db, br), 3019 (br,mult), 2652(w), 2502 (w), 2431 (br), 1607 (s), 1524 (m), 1483 (s), 1392 (w), 1359 (m), 1347 (m), 1280 (m), 1239.52 (m), 1201 (s), 1095 (w) 1035 (w, mult), 866 (m), 802 (vs), 662 (m, mult) (s = strong, m = medium, w = weak, db = double, mult = multiple, br = broad, sh = shoulder, v = very).

X-Ray Crystallography: Data collections of **1** $(H_2L)[Cu(H_2O)Cl_3]Cl$ were carried out on a Bruker D8 Venture diffractometer fitted with a Photon 100 CMOS detector employing graphite-monochromated Mo-Kα radiation, using φ and ω scans. Using the SAINT+ software,[28] the data were reduced and absorption corrections were made using SADABS.[29] Structure solution was carried out using SHELXS-97[30] while refinements were performed using SHELXL-2016.[31] Non-hydrogen atoms were refined using anisotropic thermal parameters. Hydrogen atoms were located in the lattice and refined isotropically. Hydrogen atoms attached to N21, O14, and O1 were refined using an anti-bumping restraint (0.88Å). Table 1 summarizes the crystallographic information for **1**. The data were deposited with the CCDC as deposition number 1983353.

Table 1. Crystallographic data for **1**

Formula	$C_{10}H_{12}N_2O_2Cl_4Cu$
Molecular Weight	397.57
Crystal System	orthorhombic
Space Group	*P*bca
a(Å)	6.8757(3)
b(Å)	16.2729(5)
c(Å)	25.0962(10)
α(deg)	90
β(deg)	90
γ(deg)	90
V(Å^3)	2807.95(19)
Z	8
T(K)	150(2)
ρ_{calc} (g cm^{-1})	1.881
μ(mm^{-1})	2.303
λ(Å)	0.71073
Index Ranges	$-10 \le h \le 10$
	$-23 \le k \le 23$
	$-36 \le l \le 36$
Obs. reflections	111015
Indep. Reflections [I>2σ(I)]	4278
Parameters	220
Goodness of fit	1.103
R1 [I>2σ(I)]	0.0202
R_w [I>2σ(I)]	0.0505
R1 (all reflections)	0.0243
R_w (all reflections)	0.0520

Magnetism: The magnetization of **1** was measured using a Quantum Design MPMS-XL SQUID magnetometer on powdered single-crystals (93.4 mg). Magnetization as a function of applied magnetic field from 0-50 kOe was recorded at 1.8 K. The moment was measured at several points while decreasing the magnetic field back to zero to check for the presence of hysteresis; none was observed. Temperature dependent data for **1** were measured in a 1 kOe applied field from 1.8K to 310K. The data were corrected for the temperature independent paramagnetic contribution of Cu(II) and the diamagnetic contributions of the constituent atoms (estimated from Pascal's constants[32]). Powder X-ray diffraction data were used to verify that the sample used for magnetic data collection was the same phase as the single crystal structure (see Supporting Information Section 2).

Computational studies: The magnetic susceptibility data of **1** have been calculated using a First-Principles Bottom-Up (FPBU) working strategy.[33] In brief, the FPBU procedure has been used to (i) identify all A···B radical pair candidates that might be magnetically important (threshold Cu···Cu distance 9.0Å), (ii) compute the magnetic exchange interaction J_{AB} between those selected pairs of radicals, (iii) define the magnetic topology of the crystal in terms of all significant J_{AB} interactions, and (iv) calculate the magnetic susceptibility $\chi(T)$ by means of Statistical Mechanics and compare it to the experimental data.

For the evaluation of the J_{AB} magnetic interaction between radicals, the most appropriate cluster model has to be selected to account not only for the spin carriers, but also for the radical environment. Therefore, two different types of models have been used. The first level of modeling accounts for just the $[CuCl_4(H_2O)]^{2-}$ radicals' bare skeleton, either as a dimer, trimer, or tetramer. The second level of modeling expands these bare skeleton simple models by taking into account not only nearest-neighbor (nn) $\mathbf{H_2L^{2+}}$ counterions, but also closest isolated chloride anions when necessary.[34] All J_{AB} exchange interactions have been calculated in terms of energy differences at the DFT/UB3LYP[35] level using the broken symmetry approach when appropriate.[36] Since the radicals are anions, a series of basis sets were tested in order to discriminate whether diffuse and/or polarization functions were required to correctly describe the magnetic interactions.[37] Diffuse functions are concluded to be important since the spin-carriers are anions. Therefore, all subsequent calculations were performed at all-electron 6-31+G(d) level. In addition, comparison of J_{AB} results using 6-31+G(d) and 6-31G (as a reference) basis sets shows that the use of 6-31G systematically calculates too small values for the magnetic interactions between radicals, reinforcing the importance of diffuse basis set functions. The energies for radical dimer pairs and tetrameric structures were calculated using Gaussian 09 Rev. D01.[38]

Finally, prior to calculating the magnetic properties of interest, one needs to choose a minimal set of radicals such that its repetition along crystallographic *a,b,c*-axes reproduces the magnetic topology of **1**. It thus follows that the most adequate magnetic model will include all significant J_{AB} exchange couplings in a ratio as close as possible to that found in the infinite crystal. On the basis of a regionally reduced density matrix approach,[33] the matrix representation of the Heisenberg Hamiltonian is built and fully diagonalized by using

the space of spin functions of the selected minimal magnetic model as a basis set. The resulting energy and spin multiplicity of all possible magnetic states are then used in the appropriate statistical mechanics expression[32] to obtain the macroscopic magnetic susceptibility $\chi(T)$ of **1**.

RESULTS

Synthesis: Reaction of acetic anhydride and 4-pyridone gave 1-(4'-pyridyl)pyridin-4-one dihydrate (L) in varying yield depending on the duration of the reflux. Reaction in air rather than N_2 did not affect the yield appreciably. Reaction of $CuCl_2 \cdot 2H_2O$ and **L** in HCl gave **1** in good yield (65%) as large bright green hexagonal blocks. Compound **1** was produced through the traditional slow evaporation technique even at different stoichiometries (1L : 1$CuCl_2 \cdot 2H_2O$ to 2L : 1$CuCl_2 \cdot 2H_2O$). Aqueous washes were avoided as **1** may decompose. The purity and reproducibility of **1** were confirmed using combustion analysis, IR spectroscopy and powder X-ray diffraction.

Crystal Structure of 1: The molecular unit of **1** is shown in Figure 2a. The Cu(II) distorted square pyramidal coordination sphere ($\tau_{Addison} = 0.216$)[39] is completed by the Cl3 ion which bridges neighboring Cu(II) units forming an axial-equatorial, zig-zag chain parallel to the *a*-axis, as shown in Figure 2b. The Cu1-Cl3A-Cu1A angle is 127.825(13)°. The equatorial Cu1 plane is parallel to the 012 crystallographic plane and is occupied by the H_2O molecule and three symmetry-unique chloride ions coordinating in a distorted square planar fashion (mean deviation from the plane including Cl2, Cl3A, Cl4, O1 = 0.1258 Å) with Cu1 0.2321 Å above the plane. Angles between adjacent ligands are close to 90° (see Table 2). The axial bridging chloride ion Cl3 is coordinated to Cu1 via a Jahn-Teller lengthened bond (2.7094(3) Å) as expected for a distorted square pyramidal Cu(II) ion.[40,41,42]

Chloride-bridged copper(II) chains are connected via pairs of hydrogen bonds (Cl4A…H2-O1) to inversion related neighboring chains in the *b* direction, as shown in Figure 2c. This results in honeycomb-like layers (Figure 3a) which are well-isolated from the neighboring layer ($d_{Cu\ldots Cu} =$ 11.2801(7) Å) as a result of the bulky $\mathbf{H_2L}^{2+}$ ions which stack in a V-shaped pattern between the layers (Figure 3b). The pyridine rings of the $\mathbf{H_2L}^{2+}$ ions are twisted relative to one another at an angle of 39.7° as observed previously.[23,24,25,26,43] Charge balance is attained via non-coordinated lattice chloride ions which stabilize the structure through hydrogen bonds to the pyridinium NH groups and both water and phenolic OH groups (Table 3), contributing significantly to the 3D structure of **1**. Table 3 details some of the important hydrogen bonding interactions present in **1**, specifically those which provide information regarding the superexchange discussion (vide infra).

(a) (b)

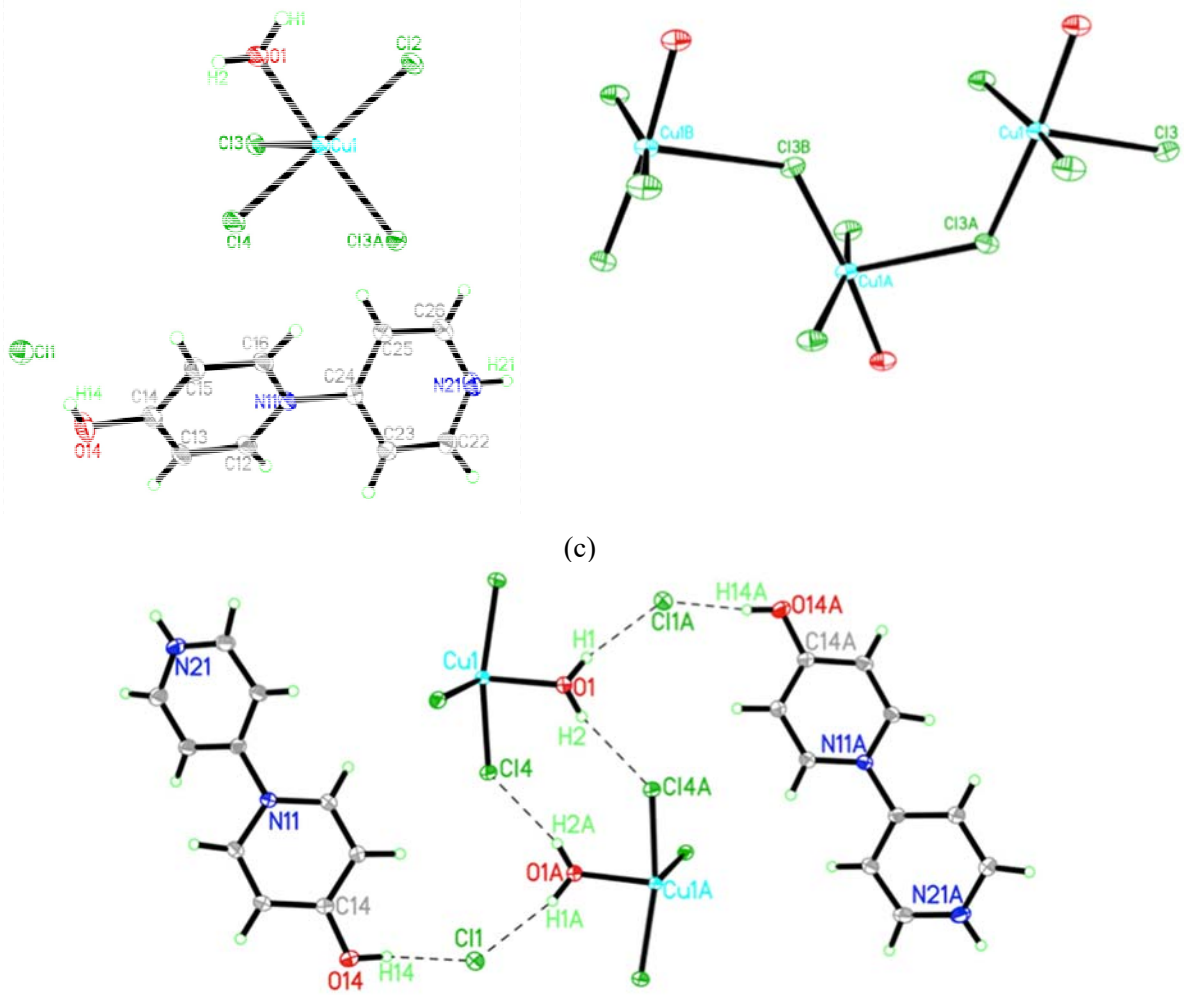

Figure 2. a) A thermal ellipsoid plot (50% probability) of the molecular unit of **1**. Hydrogen atoms are shown as spheres of arbitrary size and only N-H and O-H hydrogen atoms are labeled for clarity (Symm. Op. A: −½+x, ½-y, 1-z). b) Axial-equatorial bridging between copper(II) ions via Cl3 (Cl3A Symm Opp A: −½+x, ½-y, 1-z; Symm. Op. B: x-1, y, z). c) Hydrogen bonding observed in **1**. Equivalent species are related by inversion (Symm. Op. A: -x, -y, 1-z).

Table 2. Selected bond lengths and angles of the Cu(II) coord. sphere. (Symm. Op. A: −½+x, ½-y, 1-z)

	Bond Lengths (Å)	Bond Angles(°)	
Cu1-Cl2	2.2543(3)	O1-Cu1-Cl2	86.23(3)
Cu1-Cl3	2.7094(3)	O1-Cu1-Cl3	87.79(3)
Cu-Cl4	2.2795(3)	O1-Cu1-Cl3A	174.20(3)
Cu-O1	1.9983(9)	O1-Cu1-Cl4	88.27(3)
Cu-Cl3A	2.2757(3)	Cl2-Cu1-Cl3	102.289(11)
		Cl2-Cu1-Cl3A	91.725(11)
		Cl2-Cu1-Cl4	161.234(14)
		Cl3-Cu1-Cl3A	97.952(8)
		Cl3-Cu1-Cl4	102.28(3)

Table 3. Hydrogen Bonding Parameters (Symm. Op. A: x,y,z+1 ; B: x, y+1, z+1 ; C: −½+x, ½-y, 1-z)

donor-acceptor pair	D-H (Å)	H---A (Å)	D…A (Å)	D-H---A (Å)
O1-H1…Cl1A	0.849(15)	2.307(15)	3.1383(9)	167(2)
O1-H2…Cl4A	0.826(15)	2.309(15)	3.1094(9)	163(2)
O14-H14…Cl1	0.856(15)	2.060(15)	2.9126(10)	174(2)
N21-H21…Cl2B	0.852(15)	2.628(18)	3.2648(12)	132.5(17)
N21-H21…Cl3C	0.852(15)	2.423(16)	3.1742(11)	147.4(18)

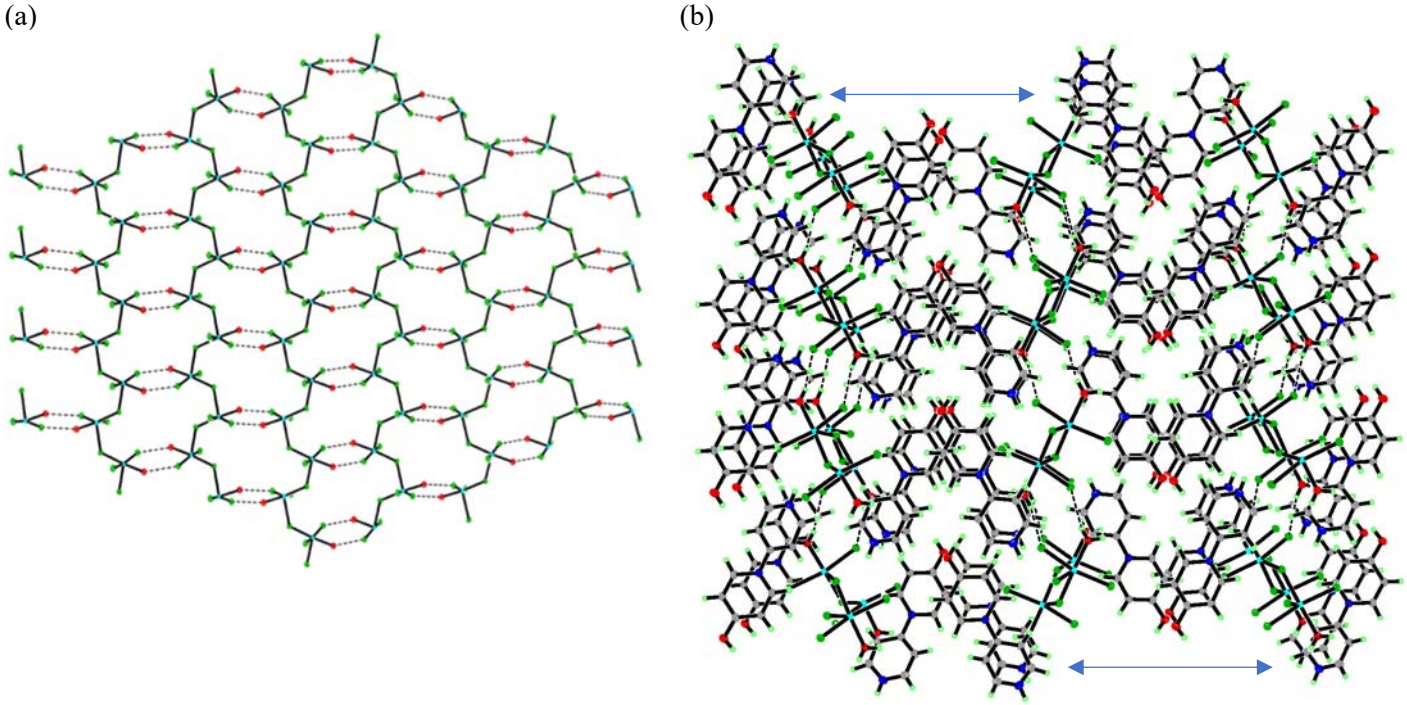

Figure 3. a) The hydrogen-bonded, chloride-bridged chains form a honeycomb-like layer parallel to the *ab*-plane (viewed parallel to the *c*-axis). Only the copper coordination sphere is shown for clarity. b) The separation between layers of hydrogen bonded copper(II) chains by the bulky cation H_2L^{2+} is shown. The two-headed arrow indicates the Cu…Cu separation.

Magnetization: The M(H) plot (Figure 4) shows a linear relationship from 0 to ~ 6 kOe and then approaches saturation as the field reaches 50 kOe where the moment reaches 65.6 emu/mol, a small fraction (~1 %) of the expected M_{sat} (~ 5,700 emu/mol for g = 2.00) for a mole of non-interacting copper(II) ions which is in good agreement with the fitted value of the paramagnetic impurity (~1.1%, Table 4, vide infra). The magnetization observed clearly corresponds to that of a trace paramagnetic impurity and indicates the presence of significant antiferromagnetic interactions and a singlet ground state in the sample.

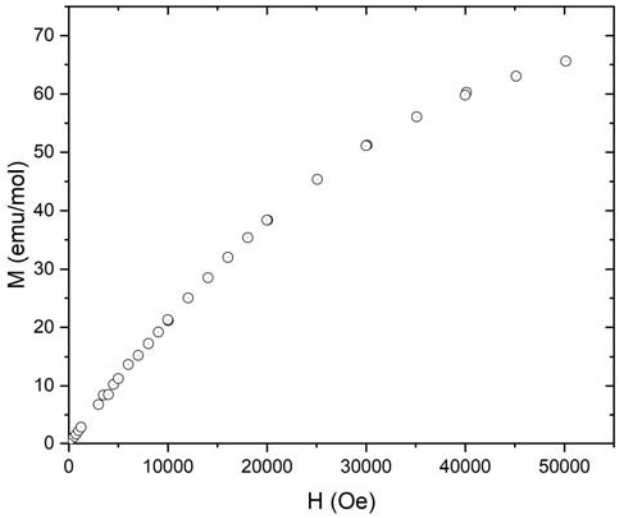

Figure 4. Magnetization as a function of field for **1** measure at 1.8 K.

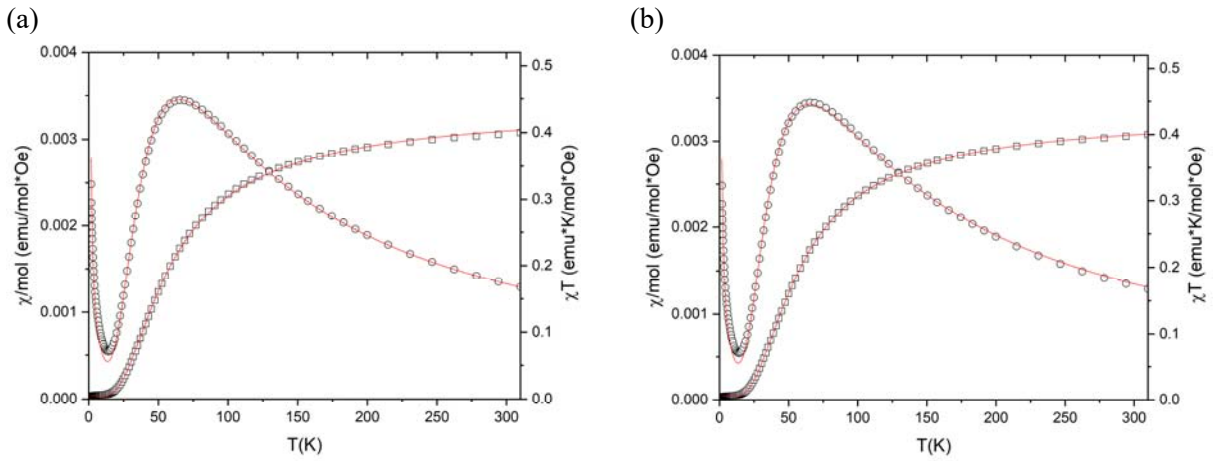

Figure 5. Susceptibility data for **1**, a) fit to the dimer model, b) fit to the strong-rung ladder model (solid lines). Left axis: χ vs. T (o) from 1.8 to 310K. Right axis: χT vs. T (□). The models include the presence of a trace paramagnetic impurity [1.12% in (a) and 1.6% in (b)].

Magnetic Susceptibility:

The magnetic susceptibility as a function of temperature from 1.8 K to 310 K in 1 kOe field is shown in Figure 5. The susceptibility increases as temperature decreases down to 67 K at which point it reaches a broad maximum at 3.4 x 10^{-3} emu/mol-Oe and then decreases as the temperature is decreased further down to 14 K (5.45 x 10^{-4} emu/mol-Oe) indicating strong antiferromagnetic interactions. The sharp increase in the susceptibility observed as the temperature is decreased further below 14 K is indicative of a slight paramagnetic impurity. Thus, the magnetic susceptibility suggests a singlet ground state in the bulk sample.

Although a uniform S = ½ chain model does not generate a singlet ground state, based on the crystal structure (see Figure 2b), attempts to fit the data to a uniform chain model were made with little success. We are unaware of an analytical model for a 2D honeycomb lattice (see Figure 3a). Therefore, the data were fit to the strong rung ladder model using an isotropic J Hamiltonian (see Eq. 1 and Supporting Information Section 3) where a negative value of J indicates antiferromagnetic interactions.[8] In this regime the axial-equatorial chloride bridged chain is easily interpreted as the ladder rail ($J_{rail} \approx$ -1 K, *vide infra*) while the hydrogen bonded dimer motif is interpreted as the ladder rung ($J_{rung} \approx$ -106 K, *vide infra*).

$$\mathcal{H} = -J\sum[S_i^x S_j^x + S_i^y S_j^y + S_i^z S_j^z] \qquad (1)$$

This approach has precedence in our group[10] and has been justified on the basis of topological similarity between the ladder and honeycomb models; both models have three nearest neighbors (nn) which may be of two different types. The strong rung ladder model parameters are summarized in Table 4. Addition of a Curie-Weiss correction parameter θ to account for interactions between motifs did not improve the quality of the fit. Attempts to employ the strong rail ladder model gave unphysical results, confirming the idea that the strong exchange occurs through the H-bonded dimers.

The Heisenberg dimer model with a Curie-Weiss correction for interdimer interactions[8] (see Eq. 2), where X= % paramagnetic impurity, CC= Curie constant, θ is the Weiss constant and J is the exchange strength (K), also gave a satisfactory fit as shown in Figure 5 and Table 4. This model suggests the axial-equatorial chloride bridged chains propagate weak exchange (θ ≈ -1 K), while the hydrogen bonded dimer interacts strongly (J ≅ -106 K). The fits to both models are acceptable; however the spin-ladder model is a slightly better fit to χT(T) (R^2 χ(dimer) = 0.99968 , R^2 χT(dimer) = 0.99989 , R^2 χ(SP ladder) = 0.98866 , R^2 χT(SP ladder) = 0.99997) (see Table 4).

$$\chi = 0.01X\left(\frac{CC}{T-\theta}\right) + (1-0.01X)\left(\frac{4CC}{3T}\right)\left(1+0.3333e^{J/T}\right)^{-1} \qquad (2)$$

Table 4. Fitting parameters for the dimer and strong rung ladder models with the standard error in parentheses. Fits to χT(T) are shown in brackets and do not include the Curie-Weiss correction θ.

Model	CC (emu-K/mol-Oe)	$J_{(rung)}$ (K)	$J_{(rail)}$ (K)	θ (K)	X (%)	R^2
Strong Rung Ladder	0.448(12) [0.4607(8)]	-105.8(7) [-106.96(16)]	2(7) [0.6(8)]	--- [---]	1.12(4) [1.42(3)]	0.98866 [0.99997]
Dimer	0.4498(7) [0.4441(5)]	-107.4(1) [-105.5(1)]	--- [---]	-1.22(3) [---]	1.61(1) [1.27(5)]	0.99968 [0.99989]

Evaluation of magnetic exchange couplings and calculation of magnetic susceptibility data

Analyzing the crystal packing (see Figure 6), we found five different pairs of $[CuCl_4(H_2O)]^{2-}$ radicals that might be magnetically significant (with Cu···Cu units within a 9.0 Å cutoff), and whose J_{AB} exchange interaction should be evaluated. The pairs of radicals are referred to as $\mathbf{d_{xy}}$, where 'xy' stands for the Cu···Cu distance. Specifically, the Cu-based dimers are 4.481 (d_{44}), 6.181 (d_{61}), 6.876 (d_{68}), 8.687 (d_{86}), 8.948 (d_{895}), and 8.993 (d_{899}) Å apart. From direct observation of the selected pairs of radicals within the crystal packing, one can immediately realize that the selected d_{xy} pairs will define (at most) a two- dimensional magnetic topology since radicals are connected along the *ab*-axes, but not along the *c*-axis (see Figure 6). Once selected, bare spin-containing units are first considered for evaluation, either as a dimer, trimer, or tetramer model. For instance, the through-bond J_{44} magnetic exchange interaction between $[CuCl_4(H_2O)]^{2-}$ radicals, which are 4.481 Å apart, has been evaluated using two, three and four radical models (see Figure 7).

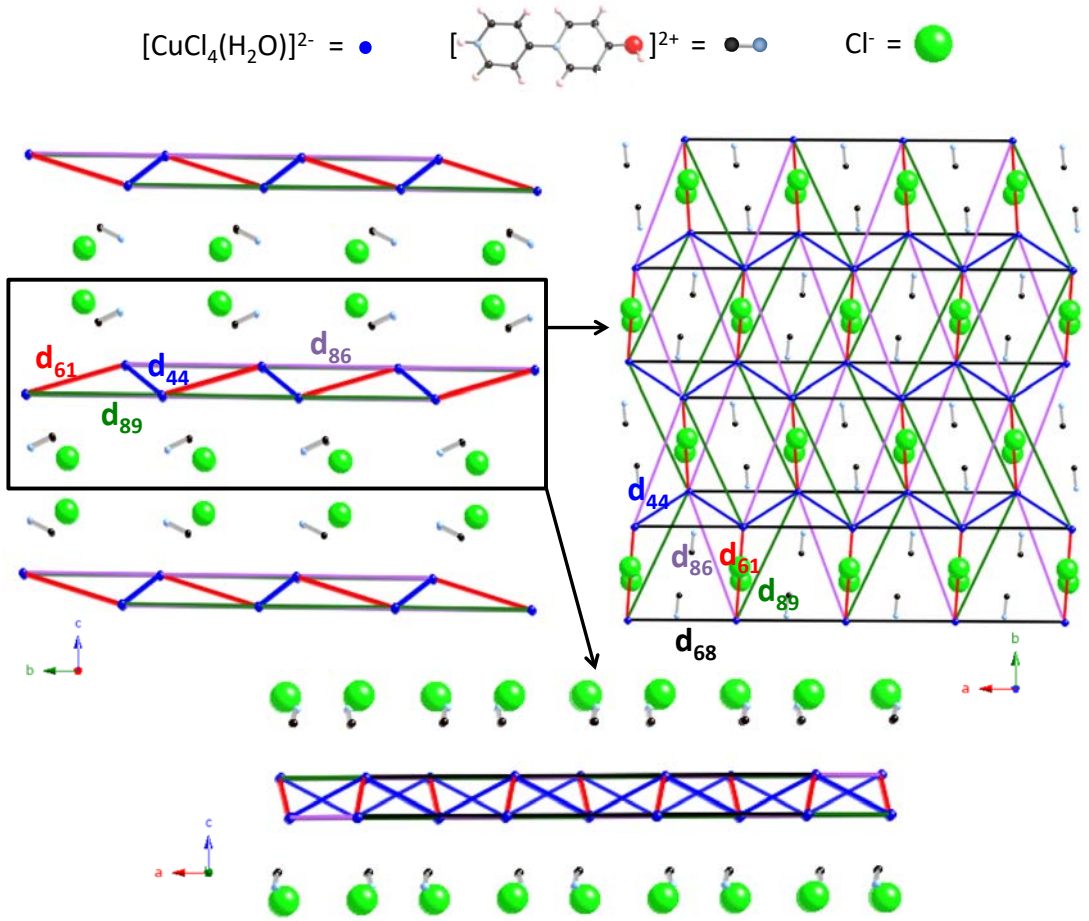

Figure 6. Schematic view along *a*-, *b*- and *c*-crystallographic axes of the crystal packing of the five pairs of $[CuCl_4(H_2O)]^{2-}$ radicals (namely, d_{44} in blue, d_{61} in red, d_{68} in black, d_{86} in purple and d_{89} in green).

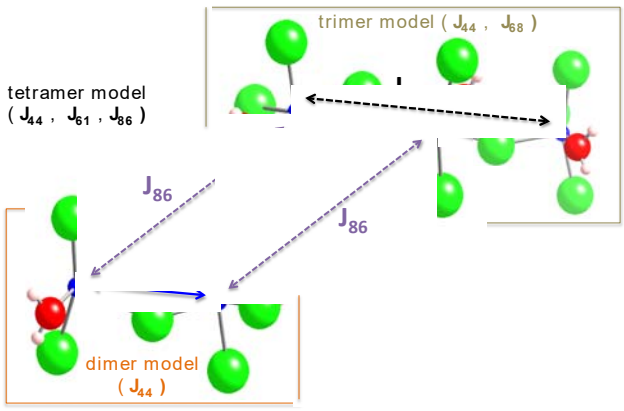

Figure 7. Dimer, trimer and tetramer bare radical skeleton models designed to evaluate J_{44} , J_{44}-J_{68} , and J_{44}-J_{61}-J_{86} magnetic interactions, respectively.

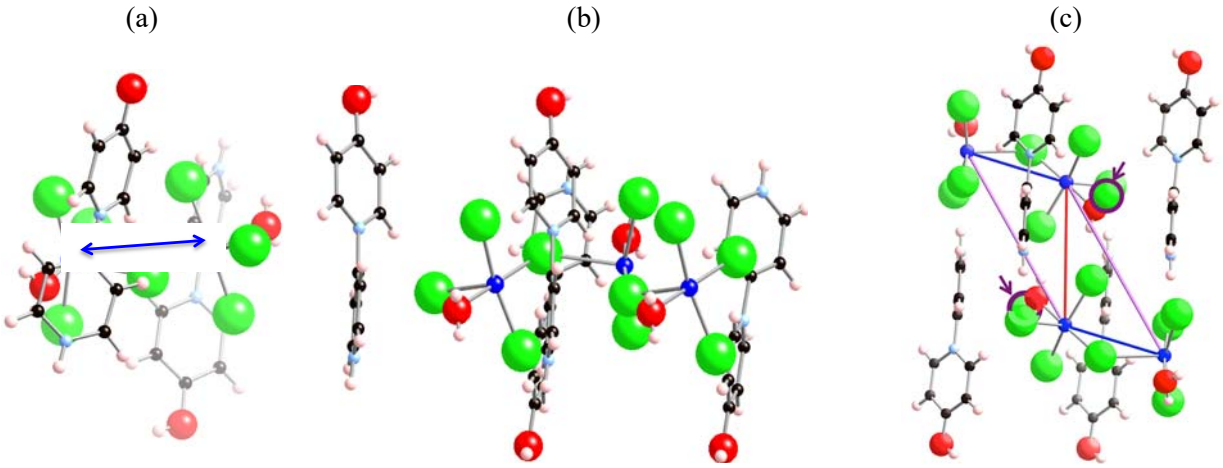

Figure 8. (a) Dimer model used to calculate J_{44} (in blue), which includes two $\mathbf{H_2L^{2+}}$ counterions. (b) Trimer model including four $\mathbf{H_2L^{2+}}$ counterions. (c) Tetramer model including four $\mathbf{H_2L^{2+}}$ counterions with and without two isolated chloride anions shown in purple (J_{44} in blue, J_{61} in red, and J_{86} in purple).

From the *ab*-view in Figure 6, one also realizes that the crystal packing of $\mathbf{H_2L^{2+}}$ counterions suggests that they might affect the magnetic interaction between most d_{xy} pairs of radicals alike. On the contrary, the J_{61} exchange interaction for d_{61} would be the most affected by the crystal arrangement of the isolated chloride anions, while J_{44} and J_{68} would be hardly affected. Clearly, the bare radical simple models must also be extended taking into account not only nearest-neighbor $\mathbf{H_2L^{2+}}$ counterions, but also the closest isolated chloride anions when necessary.

Let us remark that the trimer model in addition to J_{44} also evaluates the through-two-bonds[44] intra-chain next-nearest-neighbor J_{68} magnetic interaction. In order to study the effect of the environment in the J_{44} magnetic interaction evaluation, the dimer and trimer models have been extended including the two, and

four closest $\mathbf{H_2L^{2+}}$ counterions (nn), respectively (Figure 8a-b). Finally, a tetramer model with four counterions was evaluated together with and without two chloride anions (see Figure 8c). Besides J_{44}, all remaining magnetic interactions were evaluated using bare and extended models (see Supporting Information Section 4 for a complete account of models and a full discussion on J_{AB} evaluation).

All J_{AB} exchange interactions have been calculated in terms of energy differences at DFT/UB3LYP level (see Table 5).[35,36] It is concluded that all calculated J_{AB} values using bare radical models are underestimated at both 6-31G and 6-31+G(d) level, irrespective of using a dimer, trimer, or tetramer cluster models. This means that the environment (namely $\mathbf{H_2L^{2+}}$ nearest-neighbor (nn) counterions and isolated chloride (Cl^-) anions) must be explicitly accounted for in the cluster model employed to evaluate J_{AB} magnetic interactions.

The value of J_{44} is clearly improved when the environment is considered. Specifically, the inclusion of 2nn in the dimer model or 4nn in the tetramer model enhances the FM character of the J_{44} interaction (from 17.2 to 54.2 cm^{-1} for dimer and 14.0 to 30.6 cm^{-1} for tetramer, see Table 5).[45] Indeed, the use of counterions in a dimer model to evaluate J_{61} also enhances its FM character (see Table 5). Therefore, J_{61} is smaller in absolute value than using a bare dimer model, i.e. J_{61} becomes less AFM (from -91.8 to -77.8 cm^{-1} with 2nn to -68.4 cm^{-1} with 4nn to -34.8 cm^{-1} with 4nn and $2Cl^-$). This is exceedingly important in the tetramer model for which J_{61} varies from -102.0 to -75.4 cm^{-1} taking into account four $\mathbf{H_2L^{2+}}$ (4nn) counterions. Addition of 2 Cl^- anions does not imply significant changes in the value of J_{61} (-71.0 cm^{-1}). Nevertheless, when two chloride ions are added to the 4nn tetramer model to better describe J_{61}, one realizes that the only presence of $\mathbf{H_2L^{2+}}$ nn counterions overestimates the FM character of the J_{44} interaction (from 30.6 cm^{-1} to 17.0 cm^{-1} in Table 5). This is surprising since from direct crystal observation we had envisaged that J_{44} would not be much affected by the presence of isolated Cl^- anions. However, it is clear that the strength of the hydrogen bonds between N-atoms in $\mathbf{H_2L^{2+}}$ and nearby radicals is over-enhanced in a tetramer with 4nn model and, thus, a more complete model with 2 Cl^- is required.

The trimer model is the best model to evaluate J_{68} magnetic interactions (see trimer 4nn vs. dimer 4nn in Table 5). In fact, using a dimer model J_{68} becomes a FM interaction instead of AFM. This result is not surprising since, in the dimer models, the through-to-two-bonds[44] J_{68} interaction is considered as if it was through-space. All remaining J_{AB}'s are apparently sufficiently small to be neglected (namely, J_{86}, J_{895}, J_{899}), irrespective of the model used.

Table 5. Calculated J_{AB} exchange interactions (in cm^{-1}) using a variety of different dimer/trimer/tetramer models between Cu-radicals at 6-31+G(d) level. "Skeleton" stands for bare radical models, without counterions (nn) and chloride Cl^- anions. "Xnn" stands for models with X number of nearest-neighbor $\mathbf{H_2L^{2+}}$ counterions (nn). "XnnYCl" stands for models with X number of nn counterions and Y number of chloride Cl^- anions.

	dimer						trimer		tetramer		
	skeleton	2nn	4nn	4nn2Cl	6nn	6nn1Cl	skeleton	4nn	skeleton	4nn	4nn2Cl
J_{44}	17.2	54.2					17.2	36.6	14.0	30.6	17.0
J_{61}	-91.8	-77.8	-68.4	-34.8					-102.0	-75.4	-71.0
J_{68}	0.8		4.0				-1.2	-14.6			
J_{86}	0.0		0.0		0.0				0.0	0.2	0.0
J_{895}	0.0					0.4					
J_{899}	-0.4					30.2					

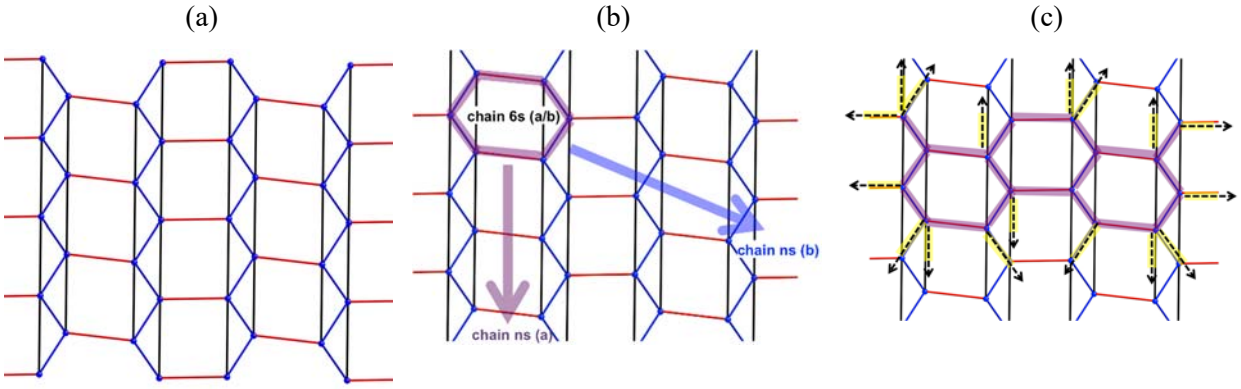

Figure 9. (a) Magnetic topology using J_{AB} calculated with dimer/trimer & tetramer/trimer models, where FM J_{44} (solid blue line), AFM J_{68} (solid black line) and AFM J_{61} (solid red line) are displayed. All $[(CuCl_3H_2O)Cl]^{2-}$ radicals have been replaced by Cu point sites (blue). (b) 6-radical honeycomb magnetic building block motif (6s) and possible extended chain and 2D magnetic models. (c) 2D cyclic 16-radical minimal magnetic model (highlighted in purple) used to reproduce the entire magnetic topology of **1**.

The calculated J_{AB}'s define a 2D honeycomb-like magnetic topology (see Table 5 and Figure 9a for *ab*-view). For either the dimer/trimer or tetramer/trimer models, there are three driving magnetic interactions: FM J_{44} and AFM J_{68} compete as a chain motif along the *a*-axis, and chain motifs are then connected by AFM J_{61} (see Figure 9a). Therefore, the magnetic topology that results from the FPBU study is a very useful tool to understand why neither a simple dimer[8] nor a strong-rung spin-ladder[8] were good fitting models to reproduce the experimental data, in spite of their good regression coefficients (Table 4).

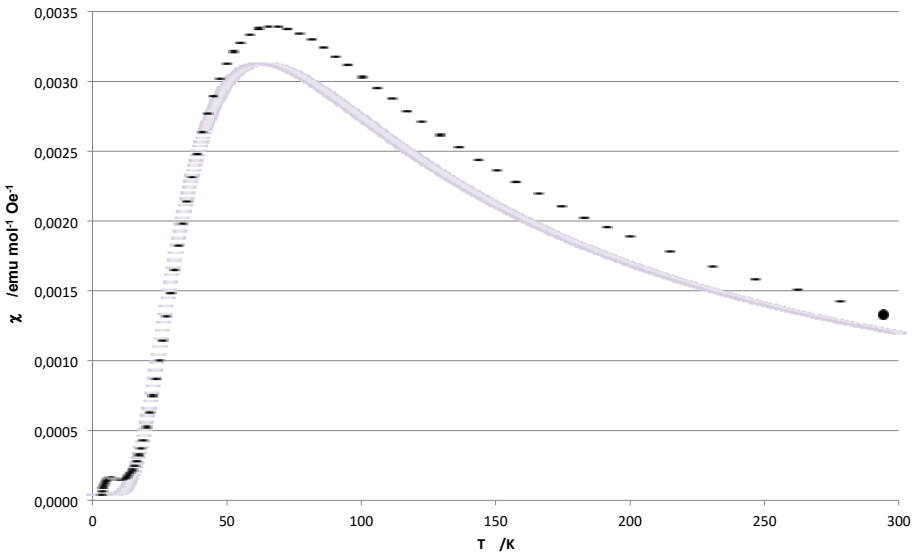

Figure 10. Magnetic susceptibility data using J_{AB} values obtained from tetramer/trimer models (J_{44}=17.0 cm^{-1}, J_{61}=-71.0 cm^{-1}, J_{68}=-14.6 cm^{-1}). Color code: experimental data in black, 16-radical 2D cyclic model in purple.

The magnetic models, which are all multiples of the 6-radical honeycomb magnetic building block motif, used to calculate the χ(T) magnetic susceptibility data include open and cyclic models to explore the cooperativity between magnetic exchange along the *a*- and *b*-crystallographic axes (see Figure 9b and Supporting Information Section 5 for a detailed discussion). Calculated χ(T) magnetic susceptibility data agree with experiment, and indicate that the 16-radical 2D cyclic model using J_{AB} from tetramer/trimer (Jt, namely, J_{44}=17.0 cm^{-1}, J_{61}=-71.0 cm^{-1} & J_{68} =-14.6 cm^{-1}) models has to be used to simulate the magnetic susceptibility of **1** (see Figure 9c for model; and purple circles in Figure 10 for χ(T) data).

The experimental magnetic susceptibility data as a function of temperature for **1** shows an increase in susceptibility to a maximum of 0.00337 emu/mol-Oe at 65.5 K with no observed increase in χT(T), which is indicative of dominant AFM interactions. At lower temperatures, χ(T) decreases rapidly toward 0, supporting the presence of AFM interactions, as well as indicating a singlet ground state. The calculated χ(T) data increase to a maximum of 0.00308 emu/mol-Oe at 59.0 K in good agreement with the experimental data. Competing FM J_{44} and AFM J_{61}, J_{68} interactions are thus found to be crucial to tune the resulting macroscopic magnetic response.

In fact, the competition between FM and AFM pair interactions leads to geometrical frustration in **1** (see Figure 11). Bearing in mind that the strong AFM J_{61} has to be always satisfied, there are two possible limiting spin arrangements depending on whether FM J_{44} (Figure 11a) or AFM J_{68} (Figure 11b) is satisfied, since the disposition of the AFM J_{61} coupled radicals is not compatible with the two remaining exchange

interactions. It is clear that fulfillment of FM J_{44} interactions introduces a higher degree of geometrical frustration (compare Figures 11a and 11b). Therefore, it is more likely that compound **1** satisfies both AFM J_{61} and J_{68} to the detriment of FM J_{44}. In any case, the possibility of exploitation of the intrinsic geometrical frustration in **1** is an advantage to further pursue investigation in this family of compounds.

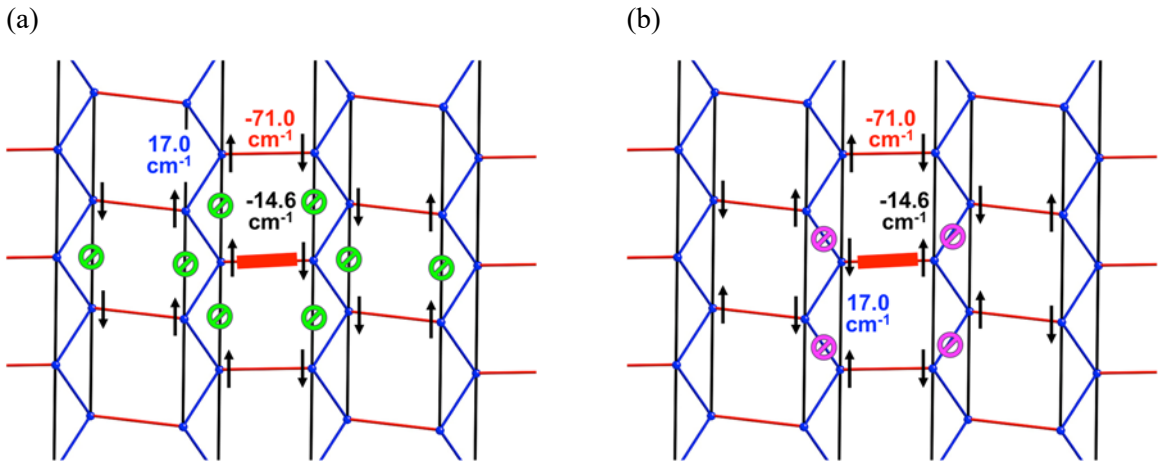

Figure 11. Spin alignment represented schematically according to: (a) AFM J_{61} = -71.0 cm^{-1} and FM J_{44} = +17.0 cm^{-1}; (b) AFM J_{61} = -71.0 cm^{-1} and AFM J_{68} = -14.6 cm^{-1}. Geometrical frustration is shown inset as green ∅ symbols in (a) and purple ∅ symbols in (b).

Magneto-structural discussion

The investigation of this lattice relies heavily on existing magneto-structural correlations. The relationship between the dimer, ladder and honeycomb models are shown in Figure 12. The strong-rung ladder and dimer models give a strong *J* coupling of *ca.* -106 K (-74 cm^{-1}) in the dimer moiety, which is unusual for the potential pathways present in **1**, namely the two-halide pathway, or the hydrogen bonded O-H···Cl pathway (see Figure 12b). Furthermore, while the strong-rung ladder model fits the data with J_{rung} and J_{rail} values similar to the dimer fit values for J and θ respectively, it is only topologically related to the honeycomb lattice and has larger residual standard deviation in the fitted parameters which suggests that the ladder model may not be appropriate for the honeycomb lattice under study in spite of prior successful use.[10]

It has been found that the axial-equatorial halide bridged chain should propagate very weak interactions in square pyramidal copper(II) complexes.[46] The Curie-Weiss correction to the dimer fit and the ladder J_{rail} is an indication of the AFM exchange strength through the mono-halide bridge (θ = -1.15K = -0.8 cm^{-1}), J_{rail} ≈ - 1 K = -0.7 cm^{-1}) coupling dimers in the layer, which agrees qualitatively with existing trends.[46,47,48] [Note: Due to differences in the Hamiltonian employed (# of nearest neighbors) and the Curie-Weiss Law, only the magnitudes of θ and J_{rail} should be compared.] The sign of the mono-halide bridged superexchange

has been related to the angle φ (Cu1-X-Cu1A) where large φ tends to give increasingly antiferromagnetic exchange while small φ gives ferromagnetic exchange.[49] However, there exists a complex (Cu(μ-Cl)(caffeine)H_2O]Cl) with weak ferromagnetic interactions (+0.5 cm^{-1}) through the same chloride bridged φ angle (128°) as **1**, and thus this relationship is tentative. Other attempts have been made to correlate structural aspects (e.g. φ/R where R = long Cu-Cl bond length, and φ = Cl-Cu-L angle where L = ligand *trans* to the bridging Cl) with the observed superexchange with only moderate success.[50] In general however these observations agree well with the orbital overlap picture between the radical containing x^2-y^2 orbital and filled d_z^2 orbital as is expected for a square pyramidal geometry involved in an axial-equatorial interaction.[48] Distortion towards trigonal bipyramidal mixes the ground state bearing the unpaired electron and thus the interaction may become stronger.

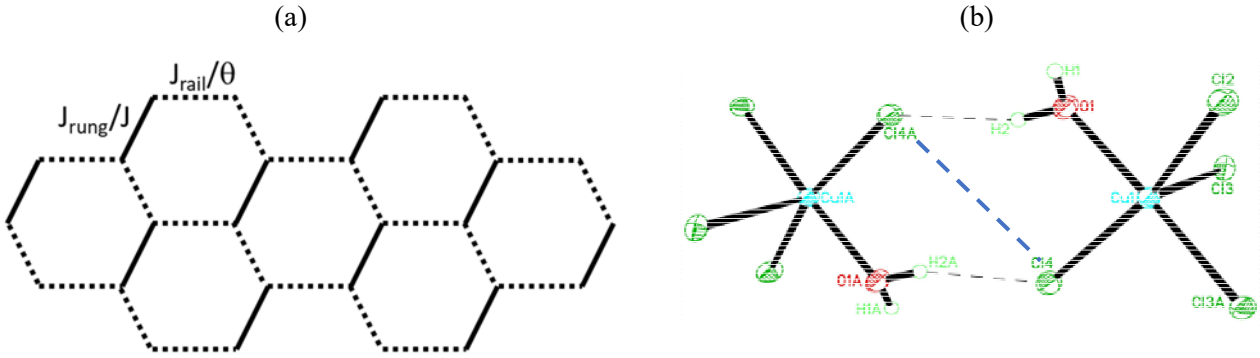

Figure 12. (a) Relationship between the honeycomb (J_{solid}, J_{dashed}), dimer (J, θ), and ladder (J_{rung}, J_{rail}) models shown diagrammatically. Note that comparison should be established between J_{solid}, J, J_{rung} and J_{dashed}, θ, J_{rail} . (b) Potential superexchange pathways present in the $[CuCl_4(H_2O)]^{2-}$ dimer moiety, indicated by dashed lines, including the hydrogen bond pathway (Cu1-O1-H2···Cl4A-Cu1A, in black) and the two-halide pathway (Cu1-Cl4···Cl4A-Cu1A, in blue).

Table 6. Details of the potential superexchange pathways within the $[CuCl_4(H_2O)]^{2-}$ dimer moiety. ∡t is the torsion angle.

Pathway	∡t°	∡Cu1-Cl4···H2A°	∡Cu1A-O1A-H2°	∡Cl4···H2A-O1A°	dCl4···H2A(Å)
Cu1-Cl4···H2A-O1A-Cu1A	168.4(3); 175.99(7)	136.1(3)	118.8(8)	163.1(10)	2.19(5)
	∡t°	∡Cu1-Cl4···Cl4A°	dCl4···Cl4A(Å)		
Cu1-Cl4···Cl4A-Cu1A	180	92.84(6)	3.9501(12)		

The often observed two-halide pathway is present in the dimer d_{61} of **1** and the parameters for both potential pathways (namely, two-halide and hydrogen bonded) are shown in Table 6 and Figure 12b. The curiously strong fitting parameter (J, J_{rung} -106 K = -74 cm^{-1}) is uncommon for either of these pathways. For instance, for the Cu-Br···Br-Cu two-bromide pathway *J* is typically in the range of 0-20 K depending on the distance between bromide ions and the angles containing the interaction.[11] However, J = -234 K (163 cm^{-1}) has been observed in (2,5-dimethylpyrazine)copper(II)dibromide.[51] Additionally, moving from the bromide to the chloride pathway in an isostructural pair typically results in much weaker exchange strengths due to the relative size of the bromide and chloride ions. In fact, Butcher *et al.*[51] suggest through density functional theory calculations that the isostructural dichloride compound with 2,5-dimethylpyrazine with a Cl···Cl distance of 3.633Å should have J = -72 K (-50 cm^{-1}). Comparison of this value to the fitting J, J_{rung} parameters of **1**, which relates to a Cl···Cl distance of 3.9501(12) Å, makes us realize that a much stronger exchange (J = -106 K = -74 cm^{-1}) is achieved using $\mathbf{H_2L^{2+}}$ as counterion.

Thus, based on existing magneto-structural correlations, the two-chloride pathway in **1** should propagate weak exchange. On the contrary, the hydrogen bonded superexchange pathway, specifically the Cu-OH···O-Cu pathway, has been recognized to have exchange strengths that typically vary greatly from very weak to strong (-94 cm^{-1})[52] and depend qualitatively on the degree of x^2-y^2 orbital overlap given by parameters such as the O···O distance and the vertical distance between copper coordination planes.[53] For **1** the relevant O···Cl distance is 3.1093(9) Å and the equatorial planes of Cu1 and Cu1A (as shown in Figure 12b and Table 6) are coincident. Given the larger size of Cl^- relative to O (~2.5x), this contact is expected to confer strong exchange since the O···X distance/sum of radii here is only 20% larger than that found for the O···O case (2.32 Å).[52] It is therefore reasonable to infer that the strong exchange is propagated via the hydrogen bonded pathway with a smaller contribution from the 2-halide pathway. These results are in complete agreement with the results of the FPBU study which support the strong exchange observed through the $[CuCl_4(H_2O)]^{2-}$ dimer moiety superexchange pathway (J_{61} = -71 cm^{-1}, see J_{solid} in Figure 12a). However, the apparent vanishingly small exchange through the single halide bridge is merely a brute average of the competing nn (FM, J_{44} = 17 cm^{-1}, see J_{dashed} in Figure 12a) and nnn (AFM, J_{68} = -15 cm^{-1}, not shown in Figure 12a) exchange interactions.

Computational results show that the magnetic topology of compound **1** is a honeycomb,[54] but no full analytical fitting honeycomb model exists. Instead dimer, with an interdimer exchange parameter, and strong-rung ladder fitting models were used. Based upon experimental data alone, there appear only a large -106 K exchange and a small/negligible -1 K exchange. Yet, again, we are fitting a distorted honeycomb system with at least three fitting parameters, based upon calculations, to models with only two fitting parameters - the dimer & strong-rung ladder models. Thus, the apparently negligible second exchange

parameter results from the accidental near cancellation of the nearest-neighbor and next-nearest-neighbor exchange interactions. In the absence of a valid analytical model for the honeycomb lattice, the models employed are the most reasonable available, but are used being fully aware that the obtained fitting parameters are estimates of the real ones.

Conclusions

The first principles bottom up study of **1** demonstrates that the environment of $[(CuCl_3H_2O)Cl]^{2-}$ radical/spin-containing units is crucial to evaluate the strength of a given radical···radical magnetic interaction. It has been disclosed that hydrogen bonding between radicals and environment (H_2L^{2+} counterions and Cl^-) enhances the FM character of pair exchange interactions in **1**.

The magnetic topology of **1** has been found to be two-dimensional (crystallographic *ab*-direction). According to the tetramer cluster model, there are two predominant competing J_{AB} interactions along the *a*-axis, namely FM J_{44} (+24.8 K = +17.0 cm^{-1}) and AFM J_{68} (−21.0 K = −14.6 cm^{-1}), which define a chain motif. These chain motifs are then connected along the *b*-axis through strong AFM J_{61} (−102 K = −71 cm^{-1}), resulting in a 2D honeycomb-like magnetic topology. It must be stressed that, although a strong-rung ladder and a dimer models can fit the experimental χ(T) data, our computational study shows that these fitting parameters carry no physical meaning since a honeycomb plaquette must be taken as magnetic building block for **1**, as was foreseen from crystal inspection. A cyclic 16-radical minimal magnetic model thus based on this honeycomb plaquette perfectly reproduces the χ(T) behavior for all range of temperatures.

Finally, it is worth mentioning that the competition between FM J_{44} and AFM J_{68} could induce interesting magnetic response at low temperatures, if the magnetic exchange is adequately tuned by modifying substituents in ligands and, in turn, interactions within the crystal packing. Besides, geometrical frustration could also be manipulated to profit from certain superexchange pathways, and thus enhance the FM interactions within this family of compounds.

Conflicts of interest

There are no conflicts to declare.

Acknowledgements

MD thanks financial support from MINECO CTQ2017-87773-P/AEI/FEDER project, Spanish Structures of Excellence María de Maeztu program through grant MDM-2017–0767, and Catalan

DURSI 2017SGR348 project. JCM, CPL and MMT are grateful for funds from PCISynthesis, Inc. (now SEQENS) toward the purchase of the X-ray powder diffractometer, the National Science Foundation (IMR-0314773) toward the purchase of the MPMS SQUID magnetometer and the Kresge Foundation toward the purchase of both.

Supporting Information. The supporting information contains 1) ^{1}H- and ^{13}C-NMR spectra of the ligand, 2) powder X-ray diffraction data of the complex compared to the calculated spectrum, 3) details of the modeling of magnetic data along with figures, and 4) detailed descriptions of the cluster models used to calculate the magnetic properties.

For Table of Contents only

Synopsis

Synthesis and characterization of $H_2L(CuCl_3H_2O)Cl$ (H_2L=*1-(4'-Pyridinium)pyridin-4-ol-ium*) reveals a chain of μ-Cl bridged $CuCl_3H_2O^{1-}$ units cross-linked by hydrogen bonds. Magnetic susceptibility measurements show a singlet ground state for the material. The unusually strong magnetic exchange across the hydrogen bonded units is supported by FPBU theoretical calculations.

ToC Graphic

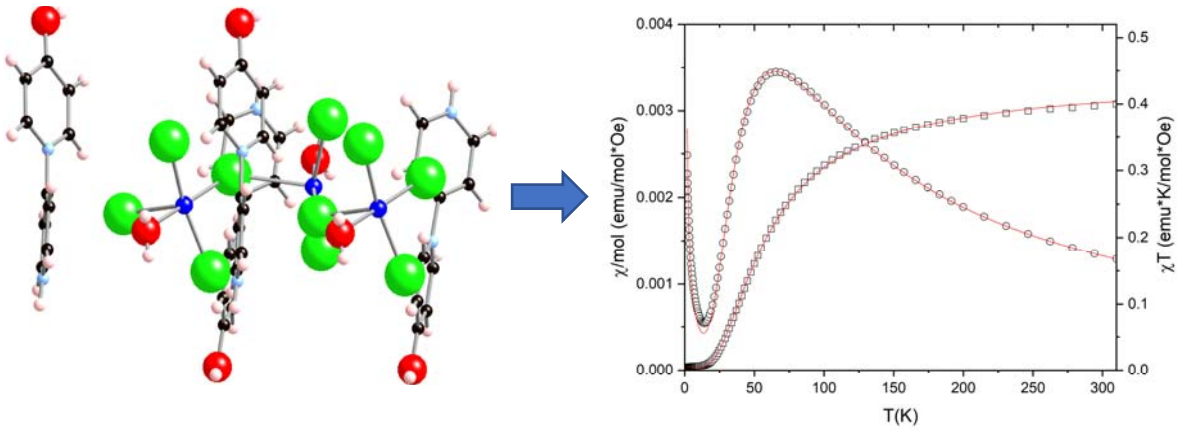

REFERENCES

[1] Manousakis, E., The spin-½ Heisenberg antiferromagnet on a square lattice and its application to the cuprous oxides. *Reviews of Modern Physics* **1991,** *63*, 1-62.

[2] Hu, J., Identifying the genes of unconventional high temperature superconductors. *Sci. Bull* **2016**, 61, 561-9.

[3] Kataev, V.; Choi, K. Y.; Gruninger, M.; Ammerahl, U.; Buchner, B.; Freimuth, A.; Revcolevschi, A., Strong anisotropy of superexchange in the copper-oxygen chains of La(14)-xCaxCu24O41. *Phys Rev Lett* **2001,** *86* (13), 2882-5.

[4] Mukuda, H.; Shimizu, S.; Iyo, A.; Kitaoka, Y., High-Tc Superconductivity and Antiferromagnetism in Multilayered Copper Oxides –A New Paradigm of Superconducting Mechanism–. *J. Phys. Soc. Jpn.* **2012,** *81*, 011008.

[5] Ralko, A.; Merino, J. Role of quantum fluctuations on spin liquids and ordered phases in the Heisenberg model on the honeycomb lattice. *Phys Rev.* **2018***, B97, 205112.*

[6] Tsirlin, A. A.; Janson, O.; Rosner, H., β-Cu2V2O7: A spin-1/2 honeycomb lattice system. *Phys. Rev. B* **2010**, *82*, 144416.

[7] Vladimirov, A. A.; Ihle, D.; Plakida, N. M., Spin excitations and thermodynamics of the antiferromagnetic Heisenberg model on the layered honeycomb lattice. *Eur. Phys. J. B* **2017,** *90*, 48.

[8] Landee, C.P.; Turnbull, M.M., Review: A gentle introduction to magnetism: units, fields, theory, and experiment. *Journal of Coordination Chemistry* **2014,** *67*, 375-439.

[9] Butcher, R. T.; Turnbull, M. M.; Landee, C. P.; Shapiro, A.; Xiao, F.; Garrett, D.; Robinson, W. T.; Twamley, B., Crystal structure and magnetism of a well isolated 2D-quantum Heisenberg antiferromagnet, (Quinolinium)(2)CuBr(4).2H(2)O, and its anhydrous form. *Inorg. Chem.* **2010,** *49*, 427-34.

[10] Li, L.; Turnbull, M.M.; Landee, C.P.; Jornet, J.; Deumal, M.; Novoa, J.J.; Wikaira, J.L. Synthesis, Structure, and Magnetic Behavior of Bis(2-amino-5-fluoropyridinium) Tetrachlorocuprate(II). *Inorg. Chem.* **2007,** *46*, 11254-11265.

[11] Turnbull, M. M.; Landee, C. P.; Wells, B. M., Magnetic exchange interactions in tetrabromocuprate compounds. *Coord. Chem. Rev.* **2005,** *249*, 2567-2576.

[12] Woodward, F.M.; Albrecht, A.S.; Wynn, C.M.; Landee, C.P.; Turnbull, M.M., Two-dimensional S=1/2 Heisenberg antiferromagnets: Synthesis, structure, and magnetic properties. *Phys. Rev. B* **2002,** *65, 144412*.

[13] Willett, R.D.; Wong, R.J.; Numata, M. Magnetic Susceptibility and EPR Study of Bis((3-alaninium) Tetrabromocuprate *Inorg. Chem.* **1983**, *22,* 3189-94.

[14] Willett, R.D.; Jardine, F.H.; Rouse, I.; Wong, R.J.; Landee, C.P.; Numata, M., Crystal structure, magnetic susceptibility, and EPR study of bis-(β-alaninium) tetrachlorocuprate(II): Spin-diffusion effects in a two-dimensional square planar ferromagnet with anisotropic and antisymmetric exchange. *Phys. Rev. B* **1981,** *24*, 5372-5381.

[15] Soos, Z. G.; McGregor, K. T.; Cheung, T. T. P.; Silverstein, A. J., Antisymmetric and anisotropic exchange in ferromagnetic copper(II) layers. *Phys. Rev. B* **1977,** *16*, 3036-3048.

[16] Willett, R.D.; Gatteschi, D.; Kahn, O. *Magneto-Structural Correlations in Exchange Coupled Systems*. Reidel Publishing, Dordrecht, Holland, 1985.

[17] Agrapidis, C. E.; van den Brink, J.; Nishimoto, S., Ordered states in the Kitaev-Heisenberg model: From 1D chains to 2D honeycomb. *Sci. Rep.* **2018**, *8*, 1815.

[18] Uematsu, K.; Kawamura, H. Randomness-induced quantum spin liquid behavior in the s =1/2 random J1-J2 Heisenberg antiferromagnet on the honeycomb lattice. *J. Phys. Soc. Jpn.* **2017**, *86*, 044704.

[19] Liu, Z.-X.; Dirac, B.N. Chiral Quantum Spin Liquids on the Honeycomb Lattice in a Magnetic Field *Phys. Rev. Lett.* **2018**, *120*, 187201

[20] Winter, S. M.; Tsirlin, A. A.; Daghofer, M.; van den Brink, J.; Singh, Y.; Gegenwart, P.; Valenti, R., Models and materials for generalized Kitaev magnetism. *J. Phys. Condens. Matt.* **2017,** *29*, 493002.

[21] Zhang, B.; Zhang, Y.; Wang, Z.; Wang, D.; Baker, P. J.; Pratt, F. L.; Zhu, D., Candidate quantum spin liquid due to dimensional reduction of a two-dimensional honeycomb lattice. *Sci. Rep.* **2014,** *4*, 6451

[22] Umadevi,B.; Stanley, N.; Muthiah, P.T.; Varghese, B. Synthesis, characterization and crystal structure of dichlorobis (N6-furfuryladeninium) copper(II)chloride. *Ind. J. Chem.* **2002,** *41A*, 737-740.

[23] Goodgame, D.M.L.; Grachvogel, D. A.; White, A.J.P.; Williams, D.J. Heterometallic Network Complexes of the ambidentate, extended-reach linear ligand 1-(4'-pyridyl)pyrdin-4-one. *Inorg. Chem.* **2001,** *40*, 6180-6185.

[24] Goodgame, D.M.L.; Grachvogel, D. A.; White, A.J.P.; Williams, D.J., Diverse polymeric metal complexes formed by the ambidentate ligand 1-(4′-pyridyl)pyridin-4-one. *Inorg. Chim. Acta* **2003,** *348*, 187-193.

[25] Goodgame, D. M. L.; Grachvogel, D. A.; Williams, D. J., Combination of weak covalent, hydrogen bonding, and Ag···π interactions in the formation of a 3D porous network $Ag(pypd)_2(ClO_4)\cdot CH_2Cl_2$ by the ambidentate ligand 1-(4′-pyridyl)pyridin-4-one. *J. Chem. Soc., Dalton Trans.* **2002,** 2259-2260.

[26] Brencic, J.V.; Ceh, B.; Leban, I. Structure of 1-(4-pyridyl)pyridinium trans-tetrachlorodi(pyridine)molybdate(III). *Acta Cryst.* **1989,** *C45*, 1144-1146.

[27] Arndt, F.; Kalischek, A. Beiträge zur Konstitution der sogenannten γ-Pyridone *Chem. Ber*. **1930,** *63*, 587-595.

[28] SAINT. Ver. 8.34A. (Bruker-AXS, 2014).

[29] Sheldrick, G.M. SADABS, University of Göttingen, Germany, 1996.

[30] Sheldrick, G.M. A short history of *SHELX Acta Cryst. A,* **2008***, 64*, 112-22.

[31] Sheldrick, G.M. Crystal structure refinement with SHELXL *Acta Cryst. C*, **2015**, *C71*, 3-8.

[32] Carlin, R. L. *Magnetochemistry*; Springer-Verlag: Berlin, 1986.

[33] (a) Deumal, M.; Bearpark, M.J.; Novoa, J.J.; Robb, M.A. Magnetic properties of organic molecular crystals via an algebraic Heisenberg Hamiltonian. Applications to WILVIW, TOLKEK, and KAXHAS nitronyl nitroxide crystals, *J. Phys. Chem. A* **2002**, *106*, 1299; (b) The regionally regionally reduced density matrix approach is based upon Malrieu, J. P.; Guihery, N. Real-space renormalization group with effective interactions, *Phys. Rev. B* **2001**, *63*, 5110-5119

[34] a) Deumal, M.; Giorgi, G.; Robb, M.A.; Turnbull, M.M.; Landee, C.P.; Novoa, J.J. The Mechanism of Magnetic Interaction in Spin-Ladder Molecular Magnets: A First-Principles, Bottom-Up, Theoretical Study of the Magnetism in the Two-Legged Spin-Ladder Bis(2-amino-5-nitropyridinium) Tetrabromocuprate Monohydrate, *Eur. J. Inorg. Chem.* **2005**, *23,* 4697-4706. b) Shapiro, A.; Landee, C.P.; Turnbull, M.M.; Jornet, J.; Deumal, M.; Novoa, J.J.; Robb, M.A. Lewis, W. Synthesis, Structure, and Magnetic Properties of an Antiferromagnetic Spin-Ladder Complex: Bis(2,3-dimethylpyridinium) Tetrabromocuprate, *J. Am. Chem. Soc.* **2007**, *129,* 952-959. c) Ref. 10. d) Jornet-Somoza, J.; Deumal, M. ; Turnbull, M.M.; Novoa, J.J. On the existence of temperature induced changes in the magnetic topology of crystals that show no first-order crystallographic phase transitions, *Polyhedron 2009*, *28,* 1965-1971. e) Jornet-Somoza, J.; Deumal, M.; Landee, C.P.; Turnbull, M.M.; Novoa, J.J., The Magnetism of (5MAP)2CuBr4 [5MAP = 5-Methyl-2-aminopyridinium]: A Quasi-2D or a 3D Magnetic System?, *Inorg. Chem.* **2010**, 49, 8017–8024.

[35] a) Becke, A.D. Density-functional exchange-energy approximation with correct asymptotic-behavior, *Phys. Rev. A* **1988**, *38*, 3098-100; b) Becke, A.D. Density-functional thermochemistry.3. The role of exact exchange, *J. Chem. Phys*. **1993**, *98*, 5648-52. c) Lee, C.; Yang, W.; Parr, R.G. Development of the Colle-Salvetti correlation-energy formula into a functional of the electron-density, *J.* Chem. *Phys. Rev. B* **1988**, *37*, 785-9.

[36]: a) Noodleman, L. Valence bond description of anti-ferromagnetic coupling in transition-metal dimers, *J. Chem. Phys*. **1981**, *74*, 5737-43. b) Noodleman, L.; Davidson, E.R. Ligand spin polarization and antiferromagnetic coupling in transition-metal dimers, *Chem. Phys.* **1986**, *109*, 131-43.

[37] a) Hariharan, P.C.; Pople, J.A. Influence of polarization functions on molecular-orbital hydrogenation energies *Theor. Chem. Acc.* **1973**, *28* 213-22. b) Francl, M.M.; Pietro, W.J.; Hehre, W.J.; Binkley, J.S.; DeFrees, D.J.; Pople, J.A.; Gordon, M.S. Self-Consistent Molecular Orbital Methods. 23. A polarization-type basis set for 2nd-row elements *J. Chem. Phys.* **1982**, *77*, 3654-65. c) Petersson, G.A.; Bennett, A.; Tensfeldt, T.G.; Al-Laham, M.A.; Shirley, W.A.; Mantzaris, J., A complete basis set model chemistry. I. The total energies of closed-shell atoms and hydrides of the first-row atoms *J. Chem. Phys.* **1988**, *89*, 2193-218. d) Petersson G.A.; Al-Laham, M.A., A complete basis set model chemistry. II. Open-shell systems and the total energies of the first-row atoms, *J. Chem. Phys.* **1991**, *94*, 6081-90. e) Rassolov, V.A.; Ratner, M.A.; Pople, J.A. Redfern, P.C.; Curtiss, L. A., 6-31G* Basis Set for Third-Row Atoms, *J. Comp. Chem.* **2001**, *22*, 976-84. f) Harharan, P.C.; Pople, J.A., *Theor. Chim. Acta* **1973**, *28*, 213

[38] Gaussian 09.D01, Frisch, M.J.; Trucks, G.W.; Schlegel, H.B.; Scuseria, G.E.; Robb, M.A.; Cheeseman, J.R.; Scalmani, G.; Barone, V.; Mennucci, B.; Petersson, G.A.; Nakatsuji, H.; Caricato, M.; Li, X.; Hratchian, H.P.;

Izmaylov, A.F.; Bloino, J.; Zheng, G.; Sonnenberg, J.L.; Hada, M.; Ehara, M.; Toyota, K.; Fukuda, R.; Hasegawa, J.; Ishida, M.; Nakajima, T.; Honda, Y.; Kitao, O.; Nakai, H.; Vreven, T.; Montgomery Jr., J.A.; Peralta, J.E.; Ogliaro, F.; Bearpark, M.; Heyd, J.J.; Brothers, E.; Kudin, K.N.; Staroverov, V.N.; Kobayashi, R.; Normand, J.; Raghavachari, K.; Rendell, A.; Burant, J.C.; Iyengar, S.S.; Tomasi, J.; Cossi, M.; Rega, N.; Millam, J.M.; Klene, M.; Knox, J.E.; Cross, J.B.; Bakken, V.; Adamo, C.; Jaramillo, J.; Gomperts, R.; Stratmann, V.G.; Yazyev, R.E.; Austin, O.; Cammi, A. J.; Pomelli, R.; Ochterski, C.; Martin, J.W.; Morokuma, R.L.; Zakrzewski, K.; Voth, G.A.; Salvador, P.; Dannenberg, J.J.; Dapprich, S.; Daniels, A.D.; Farkas, Ö.; Foresman, J.B.; Ortiz, J.V.; Cioslowski J.; Fox, D.J., Gaussian Inc.

[39] Addison, A.W.; Rao, T.N.; Reedijk, J.; Van Rijn, J.; Verschoor, G.C. Synthesis, Structure, and Spectroscopic Properties of Copper(II) Compounds containing Nitrogen-Sulphur Donor Ligands; the Crystal and Molecular Structure of Aqua[l,7-bis(*N*-methylbenzimidazol-2'-yl)-2,6-dithiaheptane]copper(II) Perchlorate. *J. Chem. Soc. Dalton Trans.* **1984,** 1349-1356.

[40] Bacci, M., Jahn-Teller effect in five-coordinate copper(II) complexes. *Chem. Phys.* **1986,** *104*, 191-199.

[41] Deeth, R. J.; Hearnshaw, L. J., Molecular modelling for coordination compounds: Cu(II)-amine complexes. *Dalton Trans* **2005,** 3638-45.

[42] Roy, S.; Mitra, P.; Patra, A.K., Cu(II) complexes with square pyramidal (N2S)CuCl2 chromophore: Jahn–Teller distortion and subsequent effect on spectral and structural properties. *Inorg. Chim. Acta* **2011,** *370*, 247-253.

[43] Monroe, J.C.; Landee, C.P.; Turnbull, M.M.; Rademeyer, M.; Copper(II) halide salts with 1-(4'-pyridinium)-pyridinium *Inorganics* **2020**, *8*, 18/1-11.

[44] J_{68} is referred as "through-two-bonds" because connects Cu(II) that belong to the same "chain" (and thus two through-bond J_{44} cooperate), while all other "through-space" interactions (namely J_{61}, J_{86}, J_{89}) connect different chains.

[45] Vela, S.; Jornet-Somoza, J.; Turnbull, M.M.; Feyerherm, R.; Novoa, J.J.; Deumal, M., Dividing the Spoils: Role of Pyrazine Ligands and Perchlorate Counterions in the Magnetic Properties of Bis(pyrazine)diperchlorate copper(II), [Cu(pz)(2)](ClO4)(2), *Inorg. Chem.* **2013**, *52*, 12923-12932.

[46] Wang, P.; Wang, Y.-Y.; Chi, Y.-H.; Wei, W.; Zhang, S.-G.; Cottrill, E.; Shi, J.-M., Synthesis, crystal structure, and magnetism of a 1-D Cu(II) chain complex with a mono-bromide bridge, *J. Coord. Chem.,* **2013,** *66*, 3092-3099.

[47] Estes, W.E.; Hatfield, W.E.; van Ooijen, J.A.C.; Reedijk, J., Magnetic Properties and Superexchange in Single Chloride-bridged Copper(II) Chain Compounds. *J. Chem. Soc. Dalton Trans.* **1980**, 2121-2124.

[48] Folgado, J.V.; Coronado, E.; Beltran-Porter, D.; Burriel, R.; Fuertes, A.; Miravitlles, C. Crystal Structures and Magnetic Properties of the Mono-p-halogeno-bridged Copper(II) Chains Cu(pcpci)X [pcpci = N-(2'-pyridylcarbonyl)pyridine-2-carboximidate, X = CI or Br] *J. Chem. Soc. Dalton Trans.* **1988**, 3041-3046.

[49] Barros-García, F. J.; Bernalte-García, A.; Higes-Rolando, F. J.; Luna-Giles, F.; Pizarro-Galán, A. M.; Viñuelas-Zahínos, E., Crystal Structure and Magnetic Exchange in the Single Chloride-Bridged Copper(II) Chain Compound [CuCl2(TzHy)] [TzHy = (4,5-dihydro-1,3-thiazol-2-yl)hydrazine]. *Z. Anorg. Allg. Chem.* **2005,** *631*, 1898-1902.

[50] Singh, R.; Lloret, F.; Mukherjee, R., Mono- and Di-chloro-bridged Discrete Dimers and Trimers and Mono-Chloro-Bridged 1D-Coordination Polymer of Copper(II). Magneto-structural Studies *Z. Anorg. Allg. Chem.* **2014,** *640*, 1086-1094.

[51] Butcher, R.T.; Novoa, J.J.; Ribas-Arino, J.; Sandvik, A.W.; Turnbull, M.M.; Landee, C.P.; Wells, B.M.; Awwadi, F.F., Strong through-space two-halide magnetic exchange of -234 K in (2,5-dimethylpyrazine)copper(II) bromide. *Chem. Commun.* **2009,** 1359-61.

[52] Bertrand, J.A.; Black, T.D.; Eller, P.G.; Helm, F.T.; Mahmoud, R., Polynuclear Complexes with Hydrogen-Bonded Bridges. Dinuclear Complex of N,N'-Bis(2-hydroxyethy)-2,4-pentanediimine with Copper(II). *Inorg Chem* **1976,** *15*, 2965-2970.

[53] Desplanches, C.; Ruiz, E.; Rodrıguez-Fortea, A.; Alvarez, S., Exchange Coupling of Transition-Metal Ions through Hydrogen Bonding: A Theoretical Investigation. *J. Am. Chem. Soc.* **2002,** *124*, 5197-5205.

[54] Li, W.; Gong, S.-S.; Zhao, Y.; Su, G., Quantum phase transition, O(3) universality class, and phase diagram of the spin-1/2 Heisenberg antiferromagnet on a distorted honeycomb lattice: A tensor renormalization-group study. *Phys. Rev. B* **2010,** *81*, 184427.